Hydropneumatic storage methodology towards a new era of hybrid energy system's efficiency and flexibility

Joao S.T. Coelho [a], Modesto Pérez-Sánchez [b,*], Oscar E. Coronado-Hernández [c], Mohsen Besharat [d], Rui-Lin Feng [e], Elias Tasca [a], Ling Zhou [e], Helena M. Ramos [a,**]

[a] Civil Engineering, Architecture and Environment Department, CERIS, Instituto Superior Técnico, Universidade de Lisboa, 1049-001, Lisboa, Portugal
[b] Hydraulic and Environmental Engineering Department, Universitat Politècnica de València, 46022, Valencia, Spain
[c] Instituto de Hidráulica y Saneamiento Ambiental, Universidad de Cartagena, Cartagena, 130001, Colombia
[d] School of Civil Engineering, University of Leeds, Woodhouse Lane, Leeds, LS2 9JT, UK
[e] University of Hohai, College of Water Conservancy and Hydropower Engineering, China

ARTICLE INFO

ABSTRACT

This research explores the link between hydropneumatic energy storage capacity and the efficiency and flexibility of hybrid energy systems in water-energy solutions. A new methodology is introduced, featuring mathematical models, experimental data collection, and hydraulic simulations using 1D and 2D CFD models for hydropneumatics modeling. A promised energy storage efficiency of around 30–50 % was obtained on a small lab scale. The optimization of hybrid systems through Solver and Python algorithms with various objective functions enables optimal design choices tailored to specific needs such as drinking water supply, irrigation, or industrial processes. Hydropneumatic vessels emerge as an effective storage solution, combining pumped storage and hydropower in one circuit. When integrated with renewable sources, such as solar (PV) and wind energy, they offer a flexible, long-lasting energy management system, applicable across different water-energy sectors to support Sustainable Development Goals. A case study with 4.8 Mm^3/year water allocation, producing 1000 MWh of hydropower and 13500 MWh of solar energy, achieved 100 % water reliability and a 25-year cash flow of 2.5 million euros.

1. Introduction

Europe has set an ambitious goal to become the first climate-neutral continent by 2050, transitioning from fossil fuels to renewable energy sources such as hydropower [1]. The European Union (EU) aims to increase the share of renewables in its energy mix to 42.5 % by 2030, up from 23 % in 2022 [2]. However, the intermittent nature of renewable sources, such as wind and solar energy, combined with unpredictable weather patterns, presents significant challenges [3]. Achieving climate neutrality will require the energy system to rapidly adapt to balance supply and demand, necessitating efficient storage and the reintegration of excess energy [4]. Currently, battery technology faces limitations, prompting the use of artificial intelligence to upgrade hydropower infrastructure. Its use is crucial to stabilize the output of renewable energy sources, thus making it feasible to integrate renewable energy

systems [5]. This transition demands substantial adaptation of energy infrastructure in the next years in terms of feasibility and sustainable development [6]. It implies new innovative solutions to address the challenges associated with renewable energy [7].

Energy storage is a critical component in the transition to renewable energy systems (RES) [8]. Solving problems of fluid flow calculations at different length scales enables the solution of different energy challenges [9]. To take advantage of their properties are scientific allies to improve the energy efficiency of processes and their storage [10]. Hydropneumatic (HP) reservoirs can efficiently store the excess generated energy by renewable systems [11]. These tanks operate as water-air batteries, using pumps and hydro turbines to transfer water uphill [12]. In this system, water-compressed air batteries are employed for energy storage; renewable energy powers water pumps that move water into hydropneumatic tanks, thereby compressing the air within them

---

[13]. The compressed air energy storage (CAES) technology then uses this stored energy by releasing the compressed air to drive water through turbines, showing efficiencies of 85 %, with an expected lifetime of around 30 years [14].

Common renewable energy storage solutions are reliable in batteries with fast degradation [15], a significant environmental impact [16], technical [17] and economical limitations [18]. A pumped-hydro storage enables no degradation cycling solution [19], it is eco-friendly and can be underground [20] or uphill with space-saving implementation, modular, scalable [21], pecs and quick to install, enabling long-duration storage [22], only by adding hydropneumatic tanks [23].

Climate change poses a significant challenge to energy grid stability and demand due to extreme weather events [24]. Transitioning from fossil fuels to low-carbon power sources is crucial for the electricity sector, enhancing grid resilience and security [25]. Flexible electricity systems and stable storage solutions are needed to support the grid and prevent renewable energy curtailment [26]. Energy storage, particularly long-duration storage, is critical for system flexibility in water systems, considering these infrastructures are high consumers of energy, which must be supplied from RES [27]. Pumped-Hydropower Storage (PHS) is the primary source of stored energy, but its deployment is not keeping pace with increased demand [28]. Governments worldwide must take action to achieve net zero ambitions and prevent grid incidents [29].

Energy storage is crucial as countries prioritize renewable energy for post-pandemic recovery plans to achieve net zero emissions [30]. The Intergovernmental Panel on Climate Change reported that over two-thirds of global greenhouse emissions come from energy generation. The global installed capacity increased to 700 GW of solar and wind installed since 2000 [31]. This significant value cannot prevent over 250 TWh of intermittent renewable electricity go unnoticed, resulting in 180 million of CO_2 emissions in 2020 [31]. Minimizing curtailment and wasted energy improves renewable generation utilization and capacity factor, leading to higher investment returns [32]. The International Renewable Energy Agency (IRENA) highlights the importance of pumped storage in balancing supply and demand, enabling reliable, low-carbon alternatives [33]. Hydropower, with a global installed capacity of over 1330 GW, plays a crucial role in renewable electricity generation [34]. The expansion of hydropower capacity, including pumped storage, is projected to be necessary for achieving energy transition scenarios and limiting temperature rises to below 2 °C [35]. The IEA Net Zero scenario predicts a doubled total hydropower capacity by 2050, adding at least 1300 GW to existing capacity [36].

Pumped-Hydropower Storage (PHS) is the world's leading energy storage technology, representing over 10 % of the total hydropower capacity worldwide and 94 % of the global installed energy storage capacity [37]. It offers a better lifetime with lifespans ranging between 50 and 100 years [38], excellent response time [39], technical readiness level [40], inertia for grid resilience [40], and specific hydropneumatic parameters [41]. Compared to other electrical storage technologies, such as Lithium-Ion Battery (Li-ion), Lead Acid Battery, Vanadium Redox Flow Battery (VRF), Compressed-Air Energy Storage (CAES), and Hydrogen Bi-directional Energy Storage System, PHS offers a better lifetime, excellent response time, technical readiness level, and grid resilience [40,41]. PHS identified potential technologies, operational framework, comparison analysis, and practical characteristics, providing useful and practical information to the energy field [42]. Integrating these clean energy systems could contribute to integrating the different targets of the sustainable development goals into the management of the energy systems [43]. The proposed solution seeks to increase a system's flexibility and reliability, making it less dependent on the electric grid. It explores a hybrid solution that maximizes clean energy usage for water and energy needs. The inherent nature of the solution demands a planned and optimized operation control strategy, contributing to water-energy balance availability, efficiency and reliability, diminishing waste and decreasing emissions covering several

targets of the sustainable development goals (SDG) [41].

The lack of an integrated hybrid energy model with hydropneumatic vessels to store energy using renewable sources was defined by Ref. [44]. This research pushes researchers to go forward with new developments. It combines solutions in a new novel integrated modelling as will be presented in the next section where the integration of the Python modelling enables the integration of a green renewable solution [45].

The research was based on the search for a clean storage system (without short lifespan and waste) to compete with the typical batteries in this important energy transition stage. The research deeply studied possible solutions how to create a new storage system based on a clean solution (i.e., hydropneumatic behaviour to reduce the volume and consequently the ground space) in small energy communities, where the volume/power of water-energy needs is reduced. The proposed procedure can also be extended to large systems, depending only on the volume of vessels and pump capacity. Hence, this study differs from existing ones due to the use of integrated modelling developed through the presentation of all mathematical formulations for hydropneumatic simulation, in terms of flow behaviour, operation under different conditions, storage capacity, and storage efficiency, when integrated into a pumped-storage system with PV Solar. It enables in reverse mode to turbine and produce energy as a back recovery renewable energy system.

In addition to reviewing the state of the art and establishing novelty, the manuscript is divided into three other parts. The second section deals with the development of the methodology in terms of hydropneumatic system formulations, photovoltaic systems, reversible pumping, as well as optimization by Solver and Python algorithms applied to hybrid solutions. It contains the computational fluid dynamics (CFD) study, as well as the description of the laboratory used. The third section deals with the results obtained in the previous sections as well as the applied solution of the hybrid model. The fourth section deals with the conclusions and future lines of research. The research is complemented with two appendices. Appendix A contains different figures and tables that support the discussion of the results. Appendix B contains all the acronyms, variables, and their units used in the research.

2. Methodology and materials

2.1. Developed methodology

The proposed research methodology is divided into four parts to create a complete hybrid energy model based on hydropneumatic vessels used as batteries to create potential energy available when the intermittent resources are not: (i) Mathematical flow characterization in pump and hydropower operation modes and of all other systems elements in 1D or/and 2D CFD models; (ii) Lab tests development about the pumped-storage capacity and efficiency; (iii) Hybrid energy solution models developed; in solver and Python, depicting a HES with PHS, as a tool to develop various power combinations to address the optimization with the integration of intermittent renewable energies, as the best sustainable and economic energy solution. This model allows analysis of the behavior and adaptability of each potential hybrid energy system, including the ability to store excess energy of wind/solar energy production in hydropneumatic vessels composed of water-air, during periods when energy demand is lower than production, and the ability to produce hydropower during periods when the demand exceeds the production. The energy sources chosen to integrate the hybrid solution have a long lifespan, which with a proper control system can be extended. The control of the system is also crucial for the high-efficiency operation of each energy source in the hybrid solution. The control system requires an independent analysis. The model restricts the operation of some energy sources to specific intervals to guarantee that they operate at the highest efficiency that is what the optimization algorithm does.

Fig. 1a presents the electric configuration for the hybrid energy solution. This shows the main components to regulate the generated energy by Maximum Power Point Tracking (MPPT) when PV systems, wind turbines and PHS are combined. Fig. 1b presents the logic sequence by which the model is designed to simulate and optimize a hybrid energy solution. First, it runs a simulation, secondly/lastly it allows it to be optimized to find suited solutions for the operation of the hybrid solution. In the simulation process, input data must be first defined, clean, and correctly allocated to each energy source, load, etc. Then the model evaluates if the primary renewable energy sources (solar and/or wind) can fulfill the energy and water needs (water needs are by default discounted from the upper reservoir). If not, it requires auxiliary energy. Additionally, the PHS system is responsible for managing the storage of water and energy production by discharge to aid in the satisfaction of energy/water needs in case the primary sources fail to do so. The auxiliary energy, either grid of batteries by default, fulfills the rest of the energy needs and powers the pumps to ensure enough water for the requirements. With the simulation setup, it is possible to proceed to the optimization, wherein single or multi-objective functions are defined, with the decision variables corresponding to multiplier factors that directly dictate the contribution of each energy source to the operation of the system. The optimization methods defined are presented further.

After the characterization of all hybrid energy systems, the optimization process runs for each water-energy need (Fig. 1), with two initial optimization formulations in Solver, for different objective functions, labelled as OPT1, and OPT2. **OPT1**: Maximize the lifetime Cash Flow; **OPT2**: Minimize the consumption of Grid Energy used for pump operation; or/and **NSGA-II** (in Python): Maximize the hydropower production and Minimize the consumption of Grid Energy used for pump operation. The Cash Flow corresponds to the difference between revenue (selling excess energy to the grid) and costs (buying energy from the grid). The NSGA-II algorithm was used to optimize the hybrid system applied to the case study, in Python, for two objective functions: Minimize grid energy for pump operation and Maximize hydropower generated. The algorithm is based on common optimization methods (gradient for a single objective and NSGA-II for two objectives). The objective functions were selected based on logical parameters that highly dictate how the system operates. These same algorithms and objective functions can be used for different systems, requiring specific modifications for each case study assembly [46].

The model manages the energy available/produced by each energy source, following a specific hierarchy. Therefore, if renewable energy is scarce due to its intermittence, the model seeks the energy deficit through other sources, such as the PHS system. With a hydropneumatic tank as a storage mechanism for the PHS system, the energy retrieved or stored inside it is deduced according to the hydraulic parameters of the hydropneumatic: head, volume capacity, enter flow, water needs or exit flow, making a water-energy balance each time step. The model possesses a hierarchal order, to prioritize renewable sources over the electric grid towards carbon neutrality of the entire system. Additionally, the model does not impose a single energy path and solution. It can evaluate each source and dictate multiple solutions, according to the optimization defined, to contribute to the load demand by the system, making it flexible and a simple approach to simulate the control strategy of complex hybrid energy systems.

The functions were chosen due to the goal of the project; to diminish grid consumption and to implement a pumped-hydro storage system. Therefore, the second objective function is reasonable to consider, as it explores the capability of the PHS system, to compare its potential to a simple pump station system. Initially, the algorithm was designed to attribute a decision variable to each hour and factor (Hydropower, Grid, and Solar), totaling around 25 thousand variables, increasing the computational time and creating an exaggerated precision. Therefore, an approximation is identical to the one used in Solver (variables allocated to periods of the day/month) to decrease the number of decision variables. Hence, 315 variables were used in the Python algorithm to
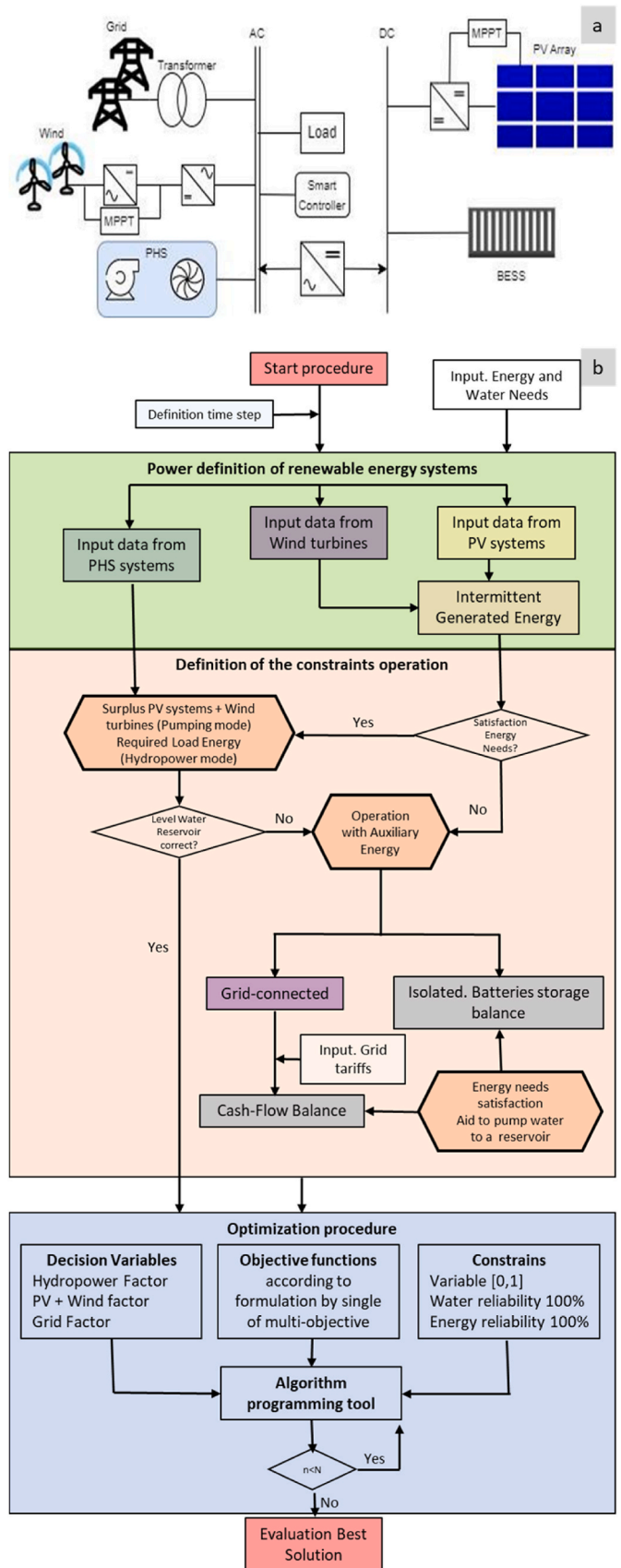
Fig. 1. General Model for a Hybrid Energy System: (a) scheme of the grid; (b) flow chart.

manipulate the energy balance during the year. A summary of the hybrid model is presented. The model receives the input data from specific energy sources, on a default hourly timestep. It then manages the energy balance between each source and their contribution to fulfilling a defined consumption (energy and/or water), respecting restrictions, such as the minimum and maximum volume of the hydropneumatic in the pump hydro storage (PHS) solution. Regarding the most complex part of the model simulation, the PHS iteration process, the feasible turbine, and the pumped volume always respect the minimum and maximum defined parameters of all system components. The optimization method serves to seek the best solutions according to the defined objective. For instance, OPT1 maximizes the lifetime cash flow, where the decision variables are multiplier factors attributed to the hydropower, pumping via solar energy and pumping via grid energy, to allow the optimization process to manage the energy balance in the best way possible. Restrictions were defined for these factors [0,1] and for the consumption needs reliability to ensure their fulfillment.

2.2. Formulations and materials

2.2.1. Flow modelling

The steady or unsteady states can be simulated using the characteristic lines are expressed as follows:

$$Q_P = C_P - C_a H_P \tag{1}$$

$$Q_P = C_n + C_a H_P \tag{2}$$

where $C_a = \frac{gA}{a}$, the acronyms list could check in Appendix B

If H and Q values are known in points A *(left)* and B *(right)* of grid points in a pipe system, then

$$C_P = Q_A \frac{gA}{a} H_A - \frac{f\Delta t}{a} Q_A |Q_A| = 0 \tag{3}$$

$$C_n = Q_B \frac{gA}{a} H_B - \frac{f\Delta t}{a} Q_B |Q_B| = 0 \tag{4}$$

Equations (3) and (4) are basic algebraic relationships that can be used to describe the transient propagation of hydraulic grade lines and water flow rates. Solving simultaneously Equations (3)–(5), the flow can be calculated along the pipe system:

$$Q_P = 0.5(C_P + C_n) \tag{5}$$

2.2.2. Hydropneumatic modelling

Hydropneumatic vessels are a versatile method for energy storage, utilizing the principles of compressible fluids like air and incompressible fluids like water or oil. The compressed gas, compressed by a pump or power source, stores potential energy in the form of pressure difference between the gas and the external environment. The energy can also be released through expansion, pushing the liquid out of the vessel, which can drive a hydraulic motor, generate electricity, or perform mechanical work. Hydropneumatic vessels can be used in water networks for smoothing pulsations, providing emergency power, or compensating for leakage. They can also be used as renewable energy storage, storing excess energy when production exceeds demand and releasing it when needed. These solutions are robust, cost-effective, and offer high round-trip efficiency, making them suitable for various energy storage needs.

Hence, by using a hydropneumatic vessel for energy storage, industries can improve energy efficiency, manage energy loads more effectively, and reduce dependence on external power sources.

Hydropneumatic reservoirs are filled by part of water and air (Fig. 2). The air can operate as a compressed air energy storage giving potential energy for the system. The mathematical formulation can be expressed as follows:

$$Q_{P,orifice} = (C_P - C_n) - (C_{a,i} + C_{a,i+1}) H_P \tag{6}$$

$$Q_{P,orifice} = C A_o \sqrt{2g\Delta H_P} \tag{7}$$

$$H_{P,air} = H_P + H_b - z_P - \Delta H_{P,orifice} \tag{8}$$

$$V_{P,air} = V_{air} - A_C(z_P - z) \tag{9}$$

$$z_P = z + 0.5(Q_{P,orifice} + Q_{orifice}) \frac{\Delta t}{A_c} \tag{10}$$

BV-01	Pneumatic Actuator Ball Valve
BV-02	Ball Valve
CV	Spring Loaded Check Valve
HT	Hydro-pneumatic Tank
DA	Data Acquisition System
HP	Compressed Air Vessel
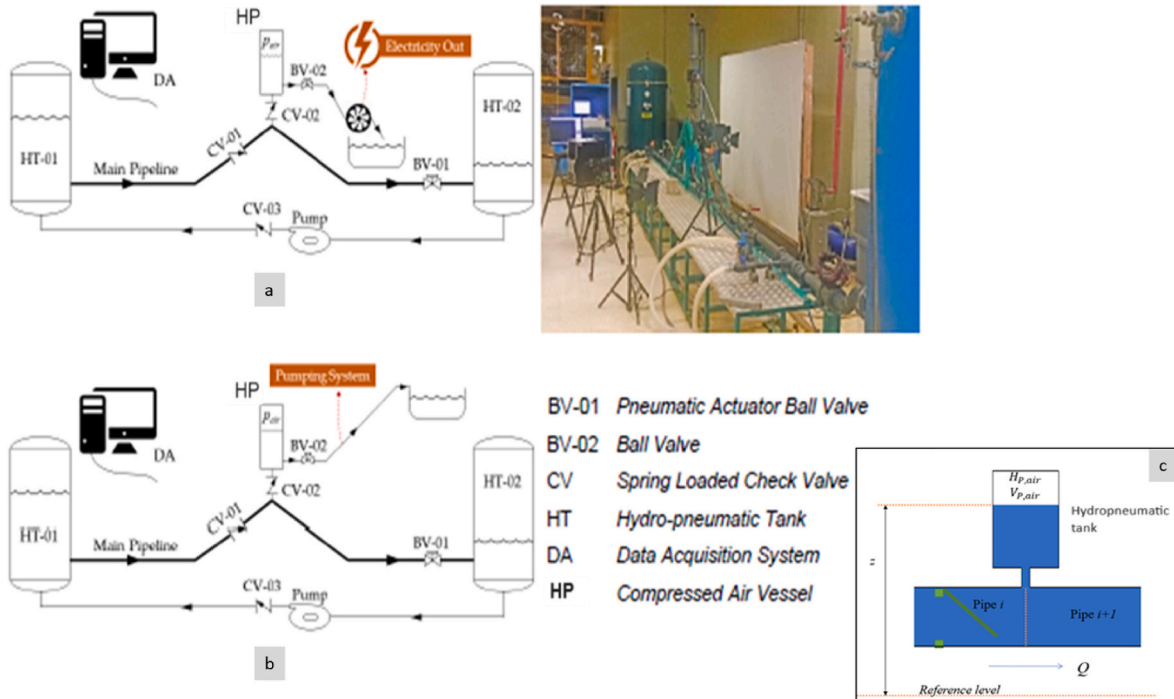
Fig. 2. Scheme of experimental hydropneumatic (HP) vessel. (a) Hydropower mode; (b) Pump mode; (c) Hydropneumatic tank.

where $H_{P,air}$ is the absolute pressure head at the end of an analyzed time step, $V_{P,air}$ is the air volume at the end of an analyzed time step, V_{air} is the air volume, $Q_{P,orifice}$ is the flow through the orifice, A_o is the cross-section of the orifice, C is the discharge coefficient of the orifice, p_c is the polytropic coefficient (usually takes a value of 1.2), z is the initial elevation of the free surface, H_b is the barometric pressure, C is the constant computed in the initial condition of the air vessel, z_p is the free surface elevation at the end of the time step, and A_c is the cross-section of the air vessel. The equation of an air vessel is obtained considering the polytropic law $\left(H_{P,air} V_{P,air}^{p_c} = C\right)$, which needs to be solved simultaneously with the following five equations.

The hydropneumatic (HP) system is used to generate energy through two approaches: electricity dispatch using a hydro-turbine and pumping system. The HP operates in two stages: water charge and discharge. In the water charge stage, the ball-valve BV-01 is actuated to induce a water hammer, causing a pressure surge [37,40]. This surge propagates in the system, causing backflow directed towards the HP. The pressure of air in the HP increases due to the compression of the air. In the water discharge stage, the compressed air expands, expelling water through the BV-02. The charge and discharge stages can be performed frequently, with 9 charge/discharge stages examined in this study, indicating a sequence of water hammer event occurrences. The HP can operate through two different approaches: the electricity dispatch system using a hydro-turbine and the pumping system.

2.2.3. Pump modelling

An analytical model characterized by mathematical equations derived from the fundamental principles of fluid dynamics and thermodynamics can predict the relationship between pressure, flow rate, efficiency, and power consumption. So based on the Method of Characteristics (MoC) or the balance of flow energy and continuity equation the steady state conditions can be simulated. In a most complete characterization based on the hydraulic grade line, the pump characteristic curve fitted by a polynomial equation depending on rotational speed, N, and characteristic lines (C_p and C_n) previously defined for the pipe flow equations, allows the following equation to estimate the pump flow (Q_p):

$$Q_P = \frac{2 - B_1 N C_a - \sqrt{(B_1 N C_a - 2)^2 - 4C_1 C_a \left(A_1 C_a N^2 + C_P + C_n\right)}}{2C_1 C_a} \quad (11)$$

where: A_1, B_1, and C_1 constants of a pump curve, and N is the rotational speed in rpm.

2.2.4. Turbine modeling

The turbine modelling can be simulated as a hydraulic dynamic orifice resistive element [21,45,47], where the head lost by the flow rate is characterized by a hydrodynamic orifice equipped with variable discharge and rotational speed coefficients as shown:

$$q_T = C_g C_s \sqrt{h_T} \quad (12)$$

where q_T is the relative flow through the turbine orifice, h_T is the relative turbine head available, C_g is the opening gate coefficient, and C_s is the runner's rotational speed coefficient.

The mathematical representation of turbomachinery parameters can be based on the specification of the relationship between flow rate Q, speed N, head H, and torque T, which are also referred to as pump characteristics. Some parameters can be defined as dimensionless values related to the point of best efficiency (also known as nominal or rated conditions) to be used as reference in different applications and the following equations [48]:

$$q = \frac{Q}{Q_R}; \ h = \frac{H}{H_R}; \ n = \frac{N}{N_R} \quad (13)$$

C_s is calculated using equation (16).

$$C_s = 1 + \frac{\alpha_R - 1}{\beta_R - 1} \left(\frac{n}{\sqrt{h}} - 1\right) \quad (14)$$

where α_R is the relative runaway discharge (Q_{RW}/Q_R), β_R is the relative runaway rotating speed (N_{RW}/N_R), n is the relative runner speed, and h is the relative turbine net head.

Assessing efficiency is a complicated task that depends on numerous parameters. The following pair of equations can be used:

$$\eta_R \frac{N}{N_R} \ for \ N < N_R \ \ C_g \left(\frac{N_{RW}}{N_{RW} - N_R} - \frac{N}{N_{RW} - N_R}\right) \eta_R \ for \ N > N_R \quad (15)$$

where N is the rotational turbine speed in rpm, and N_{RW} is the runaway rotational speed in rpm.

Equation (15) is based on turbine parameters, and it can be utilized as a dynamic boundary condition for assessing the extreme pressure occurrence in a hydropower system. Equation (16) comprises two unknowns, so another condition must be established. Assuming that the losses at the junctions between the pipe and turbine are negligible, the transient net head can be approximated by $H = H_{P,i} - H_{P,i+1}$. Considering equations of MOC, then:

$$H = \frac{C_P - Q_P}{C_{a,i+1}} - \frac{Q_P - C_n}{C_{a,i}} \quad (16)$$

The Newton-Raphson method is used to obtain Q_P as follows:

$$Q_{P,j} = Q_{P,j+1} - \frac{f\left(Q_{P,j-1}\right)}{f'\left(Q_{P,j-1}\right)} \quad (17)$$

2.2.5. CFD modeling

The transient flow modelling of a reversible hydropower system can be conducted using the Navier-Stokes equations in combination with steady-state equations as well as semi-empirical models. The numerical resolution can be performed using packages such as ANSYS, OpenFOAM, Flow3D, and FloEFD, among others. The commercial package FloEFD is a fully CAD-embedded CFD that simulates appropriately laminar, transitional, and turbulent flows. Dynamic meshes can be considered for modelling rotating components of a reversible hydropower system based on a suitable coordinate system and angular velocity. The conservation and momentum equations in the conservation form are presented below [49]:

$$\frac{\partial \rho}{\partial t} + \frac{\partial}{\partial x_i} (\rho v_i) = 0 \quad (18)$$

$$\frac{\partial \rho v_i}{\partial t} + \frac{\partial}{\partial x_j} (\rho v_i v) + \frac{\partial p}{\partial x_i} = \frac{\partial}{\partial x_j} \left(\tau_{ij} + \tau_{ij}^R\right) \quad (19)$$

where v is the water velocity in m/s, ρ is the water density in kg/m^3, and τ_{ij} is the viscous shear stress tensor in Ns/m^2. τ_{ij} is computed as (for water) [50]:

$$\tau_{ij} = \mu \left(\frac{\partial v_i}{\partial x_j} + \frac{\partial v_j}{\partial x_i} - \frac{2}{3} \delta_{ij} \frac{\partial v_k}{\partial x_k}\right) \quad (20)$$

The Reynolds-stress tensor is based on the Boussinesq assumption. τ_{ij}^R is computed as follows [50]:

$$\tau_{ij}^R = \mu_t \left(\frac{\partial v_i}{\partial x_j} + \frac{\partial v_j}{\partial x_i} - \frac{2}{3} \delta_{ij} \frac{\partial v_k}{\partial x_k}\right) - \frac{2}{3} \rho k \delta_{ij} \quad (21)$$

where μ is the dynamic viscosity coefficient in Ns/m^2, μ_t is the turbulent eddy viscosity coefficient in kgm/s, k is the turbulent kinetic energy in m^2/s^3, and δ_{ij} is the Kronecker delta function.

The $k - \varepsilon$ turbulence model has been extensively used for modelling transient flows, in which ε represents the turbulent dissipation [51]:

$$\mu_t = f_u \frac{C_u \rho k^2}{\varepsilon} \tag{22}$$

where C_u is a constant and f_u is a turbulent viscosity factor computed by:

$$f_u = \left(1 - e^{-0.0165\frac{\rho\sqrt{k}y}{\mu}}\right)^2 \left(1 + \frac{20.5\mu\varepsilon}{\rho k^2}\right) \tag{23}$$

where y is the distance from the wall.

2.2.6. Pumped-hydropower storage modeling

The Laboratory pump system was later reproduced in the hydraulic simulator model, enabling a more complex study of the pumped-storage system for comparison with the experiment tests produced in the laboratory. With this, it is possible to enhance hydraulic circuits and bypass the limitations associated with physical experiments.

The hydraulic circuit designed in WaterGEMS recreates the laboratory pumped-storage system and increments the reverse mode, i.e. hydropower, to complete the PHS system and fully analyze it. A general purpose valve (GPV) was implemented in a bypass pipeline to allow the simulation of the hydropower operation as if Pump-2 would have been replaced by a turbine. Parameters such as pipe length, material, headloss coefficients, diameter, pump characteristics, and reservoir levels were defined according to the laboratory, obtaining an almost identical virtual recreation. The pump curves provided by the manufacturer were extrapolated to the software to precisely reproduce the existing pumps as for the Pump-2.

The lower reservoir is set with an initial water level of 0.5 m and a total area of 1.606 m^2, recreating the two existing tanks in the laboratory as one single open tank in waterGEMS. The pipelines have a constant diameter of 50 mm and the same material, ductile iron (Hazen-Williams coefficient = 130). The valves used in the pump system simulation are of the "Throttle" type, which allows the regulation of the flow in the circuit and adjusts the head loss coefficient according to the closure percentage of the valves. With a flow control valve (FCV) would not have been possible to manipulate this on WaterGEMS. Both throttle control valves, BV-01 and BV-02, are configured according to the manufacturer's datasheet (Sylax DN50 Butterfly valves); using a fully open discharge coefficient of 0.0036 and a calibrated valve characteristic curve, which determines the discharge coefficient variation according to the closure percentage (Fig. 3).

The operational hydraulic circuit of the pumping system depicted in the Hydraulic CERIS laboratory serves as the basis for analysis of the pumped hydropower storage theory. Furthermore, in the hydraulic simulator, the hydropower mode (circuit's reverse direction) is additionally explored. The laboratory's pumped-storage system is limited by the lower reservoir and the hydropneumatic tank capacity. The pipeline

(a)

(b)

(c)

(d)

(e)
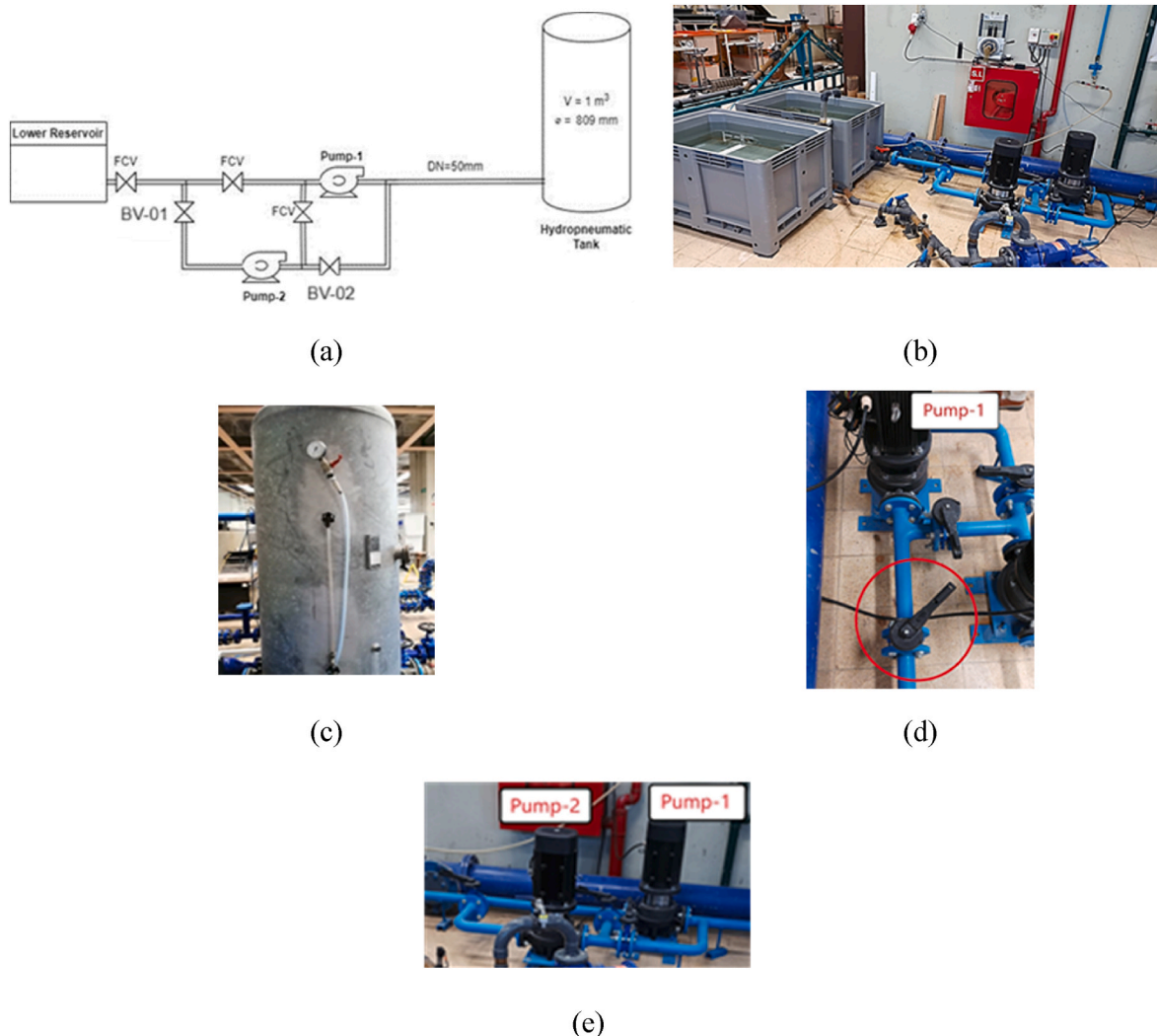
Figure 3. Laboratory's pumped-storage station: a) laboratory set-up; b) Lower reservoir + Pumps; c) Hydropneumatic vessel; d) Spherical flow control valve; e) Grundfos pumps.

is made of ductile iron ($C_{hazen-williams} = 130$) with a nominal diameter of 50 mm. Its total length via pump-1 and pump-2 is 5.1 and 6 m, respectively.

Fig. 3a presents the scheme of the lab setup. The lower reservoir, Fig. 3b, composed of two tanks, has a total area (A^{LR}) of 1.606 m^2 and a height of 0.70 m. It is elevated from the ground by 0.10 m; and the outlet pipe location, which connects the reservoir to the pumped-storage system, can be considered at the very bottom of the reservoir. The maximum volume of the reservoir is up to 0.964 m^3, nonetheless, it is sufficient for storage and steady experiments in a small defined time interval.

The hydropneumatic tank's, Fig. 3c, function is to simulate an upper reservoir of high elevation at a laboratory scale. Therefore, the hydropneumatic uses compressed air, inside its volume, to increase the hydraulic grade line at the upper tank. Table 1 presents the main characteristics of the hydropneumatic tank.

The pumped-storage system has two Grundfos pumps, of fixed rotational speed (imposed by the grid frequency), with the nomenclature/order presented in Fig. 3d and the flow control valve in Fig. 3e. Further information about the pumps' operation and characteristics is described in the next section. The pumped-storage system possesses two 4 kW Pumps from Grundfos, of fixed rotational speed. Further specifications of the pumps are presented in Table 1.

As in the laboratory experimental tests for the storage capacity. The research used WaterGEMS software [52] to simulate for the different hydraulic heads in the hydropneumatic tank, with different valve closures. The executed simulations are distinguished by the initial head in the tank, designated as H_i^{HP}, which represents the height of the water column in the tank at the beginning of the test. The values of H_i^{HP} are 5, 10, and 20 m w.c., respectively. In each head simulation, a variable closure pattern is tested, that explores the variation of flow and head losses induction on the pumping behavior.

The efficiency of the pumped-storage system and the energy stored in each trial can be evaluated based on the laboratory and simulation results. Firstly the potential energy of the water and air within the hydropneumatic tank is calculated at the start and the end of the experiment/simulation, through the following expressions, eq. (24) and eq. (25) [53]. Subsequently, the variation is derived, thereby enabling the computation of storage efficiency through the division of the potential energy delta by the total energy consumed by the pump operation.

$$E_p^w = mgh = \rho V g h = \frac{\rho g V^2}{A} \frac{1}{3.6 \, 10^6} \tag{24}$$

$$E_p^a = \frac{P \, V^{air}}{\gamma - 1} \frac{1}{3.6 \, 10^6} \tag{25}$$

Table 1
Hydropneumatic Tank Characteristics and Pumps hydraulic and electrical specifications.

Hydropneumatic Tank		Pump characteristics		Electrical Specifications	
HP Volume Capacity [m^3]	1	Pump Nominal Flow Rate [m^3/h]	31.3	Rated Power [kW]	4
Diameter [mm]	809	Nominal Head [m]	28.2	Frequency [Hz]	50
Maximum Pressure [bar]	13	Shut-off Head [m]	35.8	Rated Voltage [V]	3x 380-415
Compressed Gas	Air	Maximum Flow [m^3/h]	38	Rated Current [A]	8
		Head @Max. Flow [m]	24.3	Rated speed [rpm]	2910–2930
		Maximum Pressure [Bar] @140 °C	16	Motor Efficiency [%]	88.5

where E_p^w is the water potential energy in kWh; ρ is the water density, equal to 998 kg/m^3; g is the acceleration of gravity equal to 9.8 m^2/s; V is the water volume inside the hydropneumatic tank in m^3; A^{HP} is the bottom area of the hydropneumatic tank in m^2; E_p^a is the compressed air potential energy in kWh; P^{air} is the air pressure inside the hydropneumatic tank in Pa; V^{air} is the air volume inside the hydropneumatic tank in m^3; and γ^{air} is the heat capacity ratio equal to 1.4.

Regarding the hydropower simulation. The general purpose valve characteristic headloss curve was used to simulate the behaviour of a turbine, thus the reverse mode of pumped-hydropower storage according to Ref. [54].

3. Results and discussion

3.1. CFD analyses

2D CFD simulations have been performed to know the behaviour of all hydraulic variables and components during operation modelling in a reversible hydropower system using the OpenFoam model [55] to simulate the hydropneumatic performance. The discretization of temporal derivatives was conducted with the finite volume method in combination with a 2nd order spatial scheme. A rectangular mesh was configured with an appropriate number of cells that can represent all hydraulic phenomena.

To ensure a proper and acceptable accuracy of the results, the discretization mesh followed a typical Mesh Sensitivity Analysis (MSA), in which the density of cells is gradually increased and the solution reassessed towards an independence on the mesh size [47,49]. The discretization of the mesh was performed by assuming an initial coarse mesh with a total number of cells equal to 35,888, followed by a mesh refinement process. This process stopped when the difference in the head drop between consecutive meshes was less than 1 %, which occurred for mesh with 135,472 cells. This CFD model and 1D Method Of Characteristics (MOC) model for hydropneumatic vessels were already calibrated in previous research [47,49,54].

When the goal is to determine the flow and air pocket condition during the operational phase of the system, the 2D CFD model can provide quite appropriate results along the time in all the parts of the system geometry with about 42 h of calculation. In some cases, the 1D model is not able to predict accurately the evolution of the pressure head since it considers a constant variation of the water level at the HP. The CFD model considers all the details of the system and the initial conditions can be introduced with the highest similarity to the real model. Before presenting the CFD results, this grid independence analysis was conducted and resulted in the following choice. Mesh 3 was considered enough in terms of accuracy and computational time-consuming. It was not presented here because it was already analyzed in a previously referenced study by authors [56].

Fig. 4 shows the volume fraction and the velocity vectors during the flow establishment steps after opening the BV1. The water enters the HP when the flow is established at time 0.70 s (Fig. 4a) leading to a compression of the air pocket and increasing the pressure. The pressure suffers several changes due to the change in the flow direction towards the air vessel as shown in Fig. 4a–d. This attitude continues until a steady state flow is established in the pipe from time 1.40 s–5.90 s. During this time interval, the pressure stays almost constant in the air pocket. Upon closing the BV3 at time 5.80 s, the pressure in the air pocket rises and the air pocket size is reduced as shown in Fig. 4e and f. A vortex is shaped in the valve position in Fig. 4f with high velocity leading to perturbation of flow and very fast change in the flow regime.

The major pressure jump happens when the valve is completely closed as shown in Fig. 4g. At this moment the air pocket is in the highest compression situation with the smallest size. It leads to a very high jump in pressure. When the BV3 is completely closed, some backflow is formed mainly in the pipe upstream of the air valve and as well in the
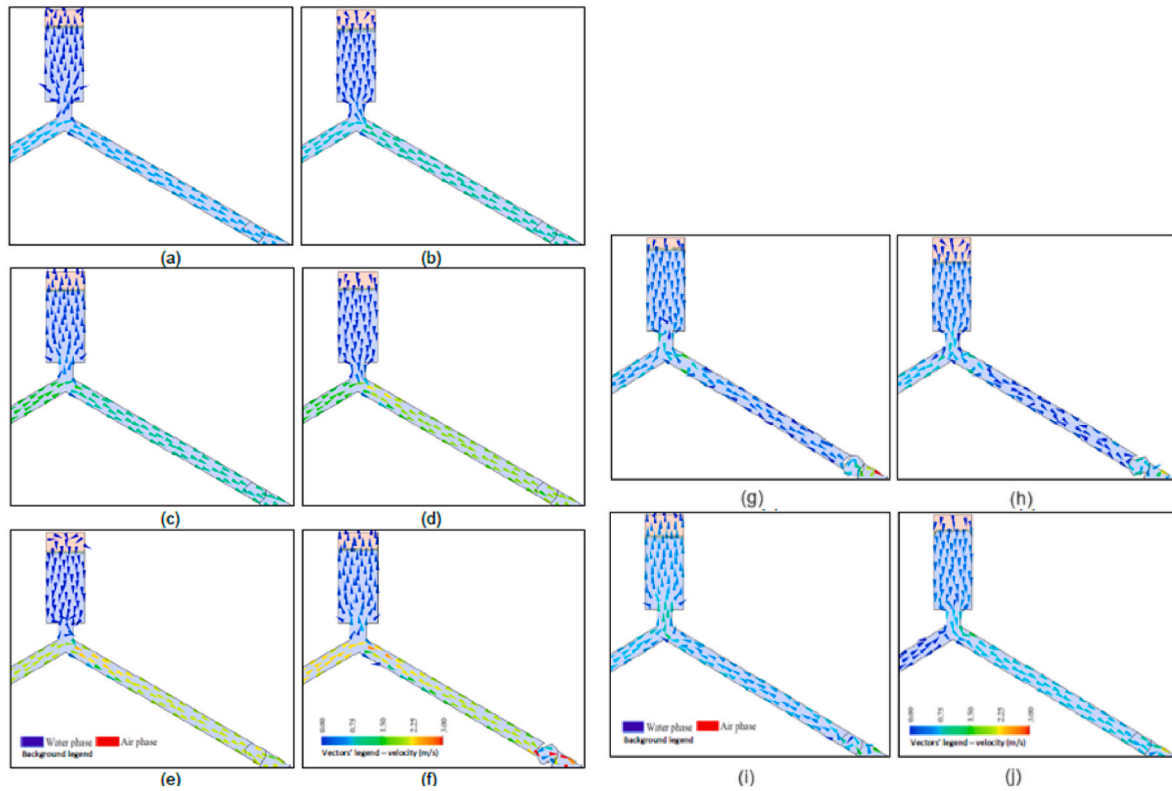
Fig. 4. Volume fraction and velocity vectors in air vessel and valve position: Left - during the pump mode: (a) t = 0.70 s, (b) t = 0.90 s, (c) t = 1.20 s, (d) t = 1.40 s, (e) t = 5.80 s, (f) t = 5.90 s. Right - during turbine mode: (g) t = 6.00 s, (h) t = 6.10 s, (i) t = 6.20 s, (j) t = 6.50 s.

near-wall zone in the downstream branch. In Appendix I, Figure A.1 represents the velocity contours and air-water interface position at HP.

3.2. Experimental storage capability values

This information is key in the simulation based on experimental results developed in the hydraulic lab, which was described in section 2.2.6. It was necessary to calibrate the pump in WaterGEMS to replicate the laboratory conditions. In the laboratory experiments, Pump-1 was singularly used, and the BV-01 valve was handled to control the flow, located upstream of the pump inlet, as shown in Fig. 3-e. The bottom reservoir, composed of two tanks with the same volume and height, has an initial water elevation of 0.5 m, to its base. For each trial, the initial hydraulic grade line (HGL) in the lower reservoir is identical; i.e. 0.5 m, excluding the difference between the floor and the base of the tanks, as the rest of the system is also located at the same height from the floor. The storage capacity test was divided into multiple trials, each with two control input parameters: initial pressure in the hydropneumatic tank and closure stage of the valve (% closure). In each trial, the valve closure percentage was fixed throughout the experiment. Table A.1 presents the registered results.

With these results, the pumped volume can be computed, plus the average flow in each trial as well. The pumped-storage system in the laboratory does not have a flowmeter, therefore the flow can only be obtained as an average, resulting from the division of the pumped volume by the measured timestamp, as described in eq. (26).

$$Q_{avg} \frac{\Delta V}{\Delta t} = \frac{A^{LR}\left(Z_i^{LR} - Z_F^{LR}\right)}{\Delta t} \qquad (26)$$

The computed values derived from the results are presented in Table A.1 in Appendix A.

The average pump head can be determined using the pump curves provided by the Grundfos manufacturer, based on the average flow rates. By considering the maximum flow rate in each trial and the flow

rate towards the end of the period, the average flow rate allows for the estimation of the pump head, pump efficiency, and pump power. With these estimated values, it is possible to calculate the total energy cost over the recorded period and divide it by the total pumped volume to assess the pump's storage capacity in kWh/m^3. Table A.2 in Appendix A summarizes the results of the storage capability tests, highlighting key parameters essential for the study of pumped-storage systems. From Table A.2, it is evident that as the average flow rate decreases, due to valve closure, the storage performance deteriorates, as the energy required to pump each cubic meter of volume increases. When the flow rate is minimal, nearly zero, the energy cost per pumped volume increases exponentially, reaching levels up to ten times higher than the average values. In Trial 1, the hydropneumatic system (HP) operates with air at atmospheric pressure. The subsequent tests involve three different hydropneumatic pressure heads, each utilizing different methods of valve closure operation.

3.3. Storage capacity of hydropneumatic air pressure variation

The storage capacity analysis compared results with the empiric parameters obtained in the CERIS/IST Hydraulic Laboratory and using WaterGEMs. In this analysis, three different hydropneumatic pressure heads were defined, each one with three different methods of valve closure operation.

Different potential energy levels within the hydropneumatic (HP) system were analyzed. For an initial head of 5 m w.c. in the hydropneumatic (H_i^{HP}) tank, the parameters over time are depicted in Fig. The evolution of the pump head and flow rate corroborates the laboratory findings, which demonstrate that the pump reaches its operational limit, preventing further volume transfer to the hydropneumatic vessel once the maximum pump head is achieved. Table A.3 provides the cumulative energy results for each valve pattern, which closely correspond to those obtained in laboratory experiments.

The laboratory circuit, modelled in WaterGEMS, shows a high degree of consistency with the experimental data, as evidenced by the calculated average parameters presented in Table A.4. For a hydropneumatic tank head of 10 m w.c., the time-dependent system curve for each valve pattern is illustrated in Figure A.3. The intersection of the pump curve with the system curve occurs at a lower initial flow rate compared to the scenario with a 5 m w.c. head. Figure A.3c demonstrates the effect of valve closure during operation, which significantly increases the head

loss coefficient, causing the system curves to approach a vertical asymptote over time. The energy results for the 10 m w.c. head in the hydropneumatic vessel are summarized in Table A.5, with the computed average hydraulic parameters in Table A.6, both showing strong alignment with experimental data.

At a head of 20 m w.c., the pump is unable to deliver additional flow due to its 36 m head limit. The system curve starts at a higher point with a lower initial flow rate, as shown in Fig. 5, which also illustrates the
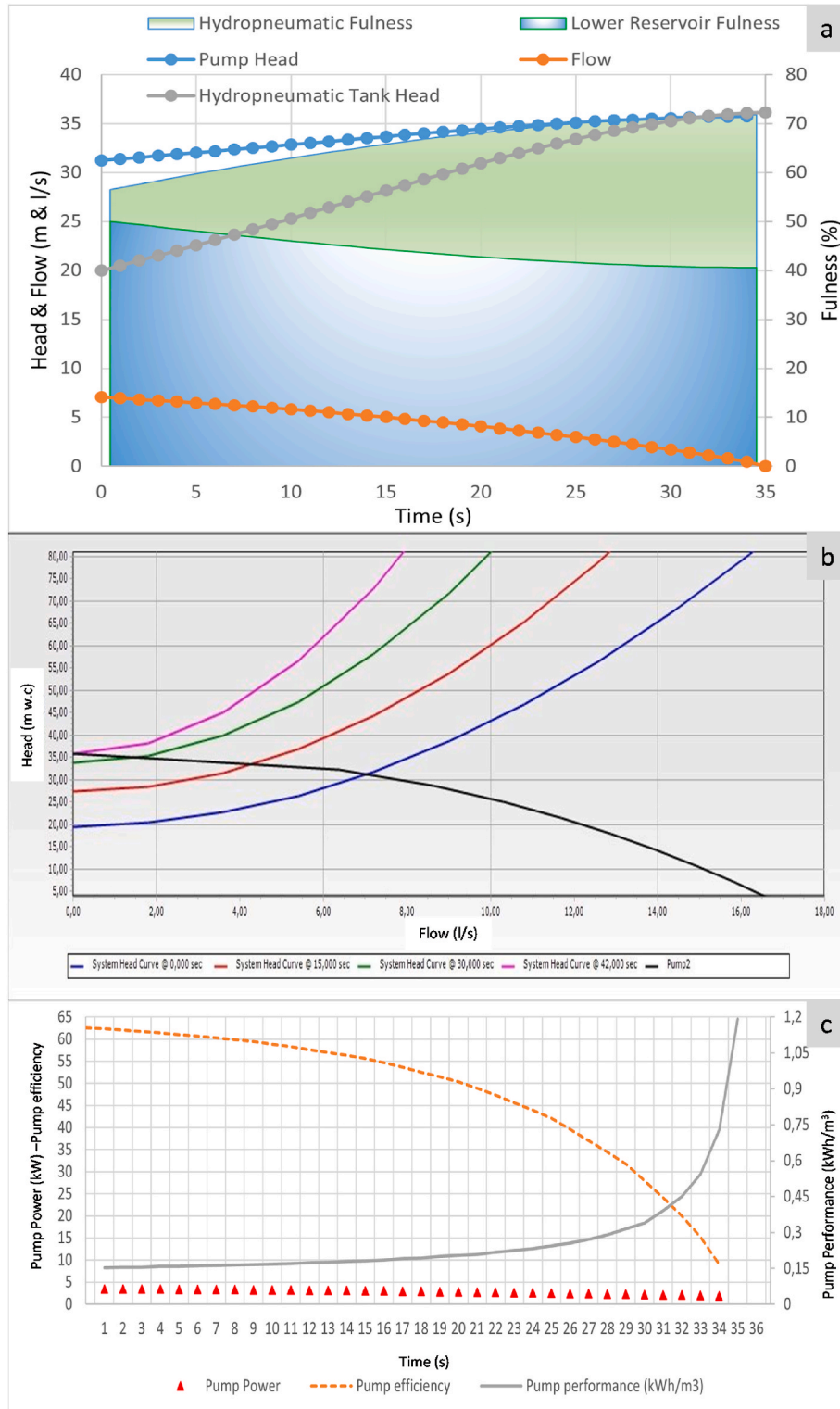
Fig. 5. (a) Circuits evolution for $H_i^{HP} = 20$ m w.c.; (b) System curve evolution for $H_i^{HP} = 20$ m w.c.; and (c) pump's performance through time for $H_i^{HP} = 20$ m w.c.

increasing verticality of the system curves as valve closure and head losses rise. The pump's energy performance and average hydraulic parameters are summarized in Tables A.7 and A.8.

3.4. Energy storage efficiency

The potential energies obtained for each trial, and the resultant energy stored in the hydropneumatic vessel are presented in Table 2, where E_p^w is the water potential energy in kWh and E_p^a is the compressed air potential energy, in kWh, with i and f are the initial and final duration registered time. The final column presents the storage efficiency of each trial, dividing the stored energy by the energy consumed by the pump.

In WaterGEMS, the precision at which the pump surpasses its maximum operating head, resulting in zero flow, is significantly higher compared to measurements taken in the lab due to pressure fluctuations. As a result, the valve closure pattern does not influence the evaluation of potential energy, with variations occurring only between different hydropneumatic head simulations. However, the pump's energy consumption does vary depending on the valve pattern, which in turn affects storage efficiency. On average, the absolute deviation between the simulation and empirical efficiencies is 2.46 %. This small deviation is primarily due to the simulation energy results being calculated using total incremental values, while the storage efficiencies derived from laboratory trials are based on average power results and the duration of each experiment. Additionally, the volume calculations in the hydropneumatic vessel for experimental analysis were based on measured heights in the laboratory. Nevertheless, the energy results and efficiencies obtained from both the simulations and experiments closely align, highlighting the technical and economic viability of energy production. This alignment also underscores the potential for highly efficient energy utilization when combined with other available renewable resources.

3.5. Hybrid model application

The hybrid energy system model integrates solar, wind, and auxiliary options with a Pumped-Hydropower Storage (PHS) system to optimize

Table 2
Laboratory and simulation energy storage results.

Trial Lab	E_i^w [kWh]	E_f^w [kWh]	E_i^a [kWh]	E_f^a [kWh]	E_{stored} [kWh]	$\eta_{storage}$ [%]
1	0.00163	0.00413	0	0.0273	0.0298	57.1
Hydropneumatic Tank at H$P \sim 5m$						
2 (0 %)	0.00160	0.00365	0.0156	0.040	0.0265	49.6
3 (34 %)	0.00185	0.00402	0.0142	0.0303	0.0183	33.9
4 (67 %)	0.00185	0.00216	0.0142	0.0188	0.00491	7.8
Hydropneumatic Tank at H$P \approx 10m$						
5 (0 %)	0.00163	0.00315	0.0310	0.0538	0.0243	46.7
6 (34 %)	0.00185	0.00345	0.0285	0.0453	0.0184	39.6
7 (67 %)	0.00175	0.00190	0.0295	0.0333	0.00395	8.3
Hydropneumatic Tank at H$P \approx 20m$						
8 (0 %)	0.00145	0.00220	0.0660	0.0813	0.0161	41.8
9 (34 %)	0.00145	0.00215	0.0660	0.0845	0.0192	29.2
Simulation HP	E_i^w [kWh]	E_f^w [kWh]	E_i^a [kWh]	E_f^a [kWh]	E_{stored} [kWh]	$\eta_{storage}$ [%] - 0 %/34 %/Var.
5m	0.00169	0.00390	0.0139	0.0345	0.0228	51.9/ 40.0/ 49.6
10m	0.00169	0.00348	0.0286	0.0459	0.0191	46.6/ 37.5/ 43.4
20m	0.00169	0.00272	0.0582	0.0689	0.0117	37.7/ 29.3/ 33.4

water and energy management, crucial for both urban and rural sectors. The model, shown in Fig. 1, supports various configurations, including renewable energy sources with or without grid and battery support. An extensive analysis using Solver optimization methods, GRG Nonlinear with the multistart feature, was conducted to compare different approaches for water-energy allocation. The system can be self-sustainable for lower water-energy demands without relying on grid energy. Table 3 presents the total results for an average year, for a certain value of water allocation (4.8 Mm^3), with a lifetime of 25 years of cash flow. The lifetime cash flow considers no selling excess of PV solar to the grid in the first five years due to government restrictions. The optimization methods yielded nearly identical results, with both approaches maximizing hydropower generation and using no grid energy due to sufficient hydropower and solar energy. OPT1 slightly increased profit by selling excess solar energy, while OPT2 showed minor differences for 4.8 Mm^3 water allocation. Both optimizations met energy and water needs efficiently.

Fig. 6 shows the 24-h energy balance, highlighting the harmonious operation of renewable subsystems to meet water-energy needs. At night, hydropower covers energy demands, while solar energy takes over during the day. The "Energy Deficit" remains zero, indicating no need for grid energy, while excess solar energy is sold as "Energy Surplus," particularly at midday.

Fig. 7-b shows a high solar surplus sold due to reservoir volume limits, preventing additional water pumping. The reservoir's hourly storage level significantly impacts the system's energy balance. Fig. 7-a highlights the interplay between solar generation, reservoir levels, and pumped volumes in the OPT1 method, which maximizes lifetime cash flow. All optimization methods achieved 100 % water reliability, ensuring 24-h irrigation for any water allocation, including 4.8 Mm^3, across the entire season. The study emphasizes the importance of meeting both water and energy needs for irrigation, drinking water supply, or industrial processes. Fig. 7-b's pie chart illustrates the energy contributions from solar, hydropower, and grid sources in the hybrid energy system.

Finally, the yearly energy balance is shown in Fig. 7b, for the case of lifetime cash flow maximization (OPT1). For 4.8 Mm^3, this optimization configuration presents the best solution, as for energy parameters, all methods have identical results, but, ultimately, this obtains the best cash flow. "Grid In" corresponds to energy sold to the grid and "Grid Out" to energy purchased from the grid. Fig. 7c and d shows the distribution of power according to source.

The yearly energy and water volume balance using the Solver or Python models with OPT1 (Fig. 7e) and OPT2 (Fig. 7f). The main differences are in the Energy Sell to the Grid, the use of PV energy for PHS in pumping mode, the top reservoir fullness that allows to allocation of the water needed, and the use of PHS in turbine mode. Depending on the objective function previously defined the complete models (Solver or Python) developed can get results to fit the best economical solution, the maximum hydropower operation, the lower carbon footprint, or others.

4. Conclusions

A new pumped-hydropneumatic storage technology has been

Table 3
Technical-economic results.

Optimization method:	OPT1	OPT2
Turbine Volume [m^3]	6,503,314.808	6,503,314.8
Pumped Volume [m^3]	11,553,481.9	11,553,941.6
Hydropower [kWh]	1,077,716.3	1,077,716.3
Solar Energy for Pump [kWh]	5,249,196.2	5,249,405.0
Grid Energy for Pump [kWh]	0.0	0.0
Grid Energy [kWh]	0.0	0.0
Solar Excess to Grid [kWh]	8,335,480.0	8,335,271.0
Lifetime Cash Flow [€]	2,527,096.0	2,477,787.0
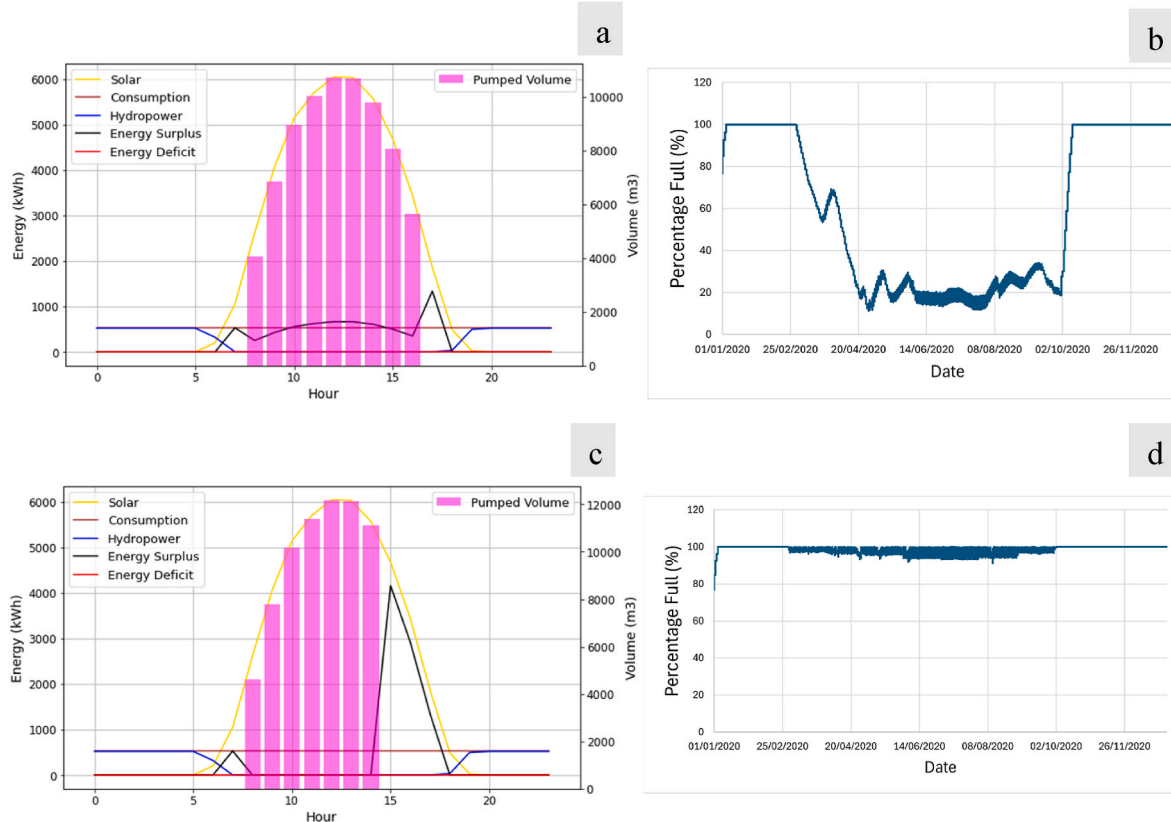
Fig. 6. Hybrid energy solution analysis: (a) OPT1. Energy Balance on 1st of August (a) and reservoir capacity throughout the year (b) for 4.8 Mm³; (b) OPT2. Energy Balance on 1st of August (c) and reservoir capacity throughout the year (d) for 4.8 Mm³.

integrated with other renewable energy sources, including PV solar, wind, the grid, and batteries. A promised energy storage efficiency of around 30–50 % was obtained on a small lab scale. The optimization hybrid model was developed using Solver and Python, allowing enhanced hybridization with pneumatic vessels as upper reservoirs. While Solver is limited to non-linear and evolutionary optimization methods, Python enables the application of multiple optimization algorithms. The methodology involved integrating physical and mathematical modelling, experimental tests, and efficiency characterization, leading to a hybrid model applied in a real case study. The system's versatility was demonstrated through 1D and 2D flow models that characterized flow behaviour in hydraulic circuits during energy production.

The study explored the energy storage capacity of a hydropneumatic (HP) system, demonstrating promising results for integrating intermittent renewable sources with pumped-hydropower storage (PHS). The HP system operates in two modes: hydropower, using available water, and pumping, using compressed air. The model was applied to a real-world scenario, ensuring water allocation and enabling energy storage from PV solar surplus, which powers a pumping station and compresses air in the HP vessel. This stored energy is later released in hydropower mode when PV energy is unavailable. Two optimization strategies identified the most cost-effective design solutions.

A real application of all models was developed for a system with water-energy nexus needs, in particular, to guarantee a water allocation from the hydropneumatic vessel of 4.8 Mm³ per year, more distributed between March and October. The potential energy guaranteed by HP, combined with a pumped-hydropower storage solution to integrate PV solar, turned the system based on an energy grid into a hybrid renewable solution, allowing energy storage in the HP vessels, whenever there is a surplus of PV Solar. This energy surplus feeds the pumping station to pump water to the water needs and the HP, compressing the air inside it,

and increasing its potential energy to be released in hydropower mode when energy is needed and PV is not available. Two optimization solutions based on two different objective functions allowed us to define and select the best technic-economic design solution. The solution obtained allows a turbine volume in an average year of 6500 Mm³ and a Pump Volume of 11500 Mm³, producing hydropower and Solar energy of 1000 MWh and 13500 MWh, respectively with 100 % water reliability, ensuring 24-h irrigation for any water allocation with a lifetime (25 years) cashflow of 2.5 M€.

Limitations of the research included the single hydraulic circuit, which prevents simultaneous pump and turbine operation, and the absence of characteristic curves for hydropneumatic energy storage capacity and performance under varying conditions and sizes, as these depend on specific system objectives. Additionally, control and electronic simulation analysis were not part of this study. Future research should focus on optimizing multi-circuit models, characterizing efficiency curves for diverse water-energy needs, and integrating control systems. Expanding the modularity and scalability of the hydropneumatic system, exploring new renewable integrations, and assessing its sustainability across various environments will enhance its viability as a long-term energy storage solution.
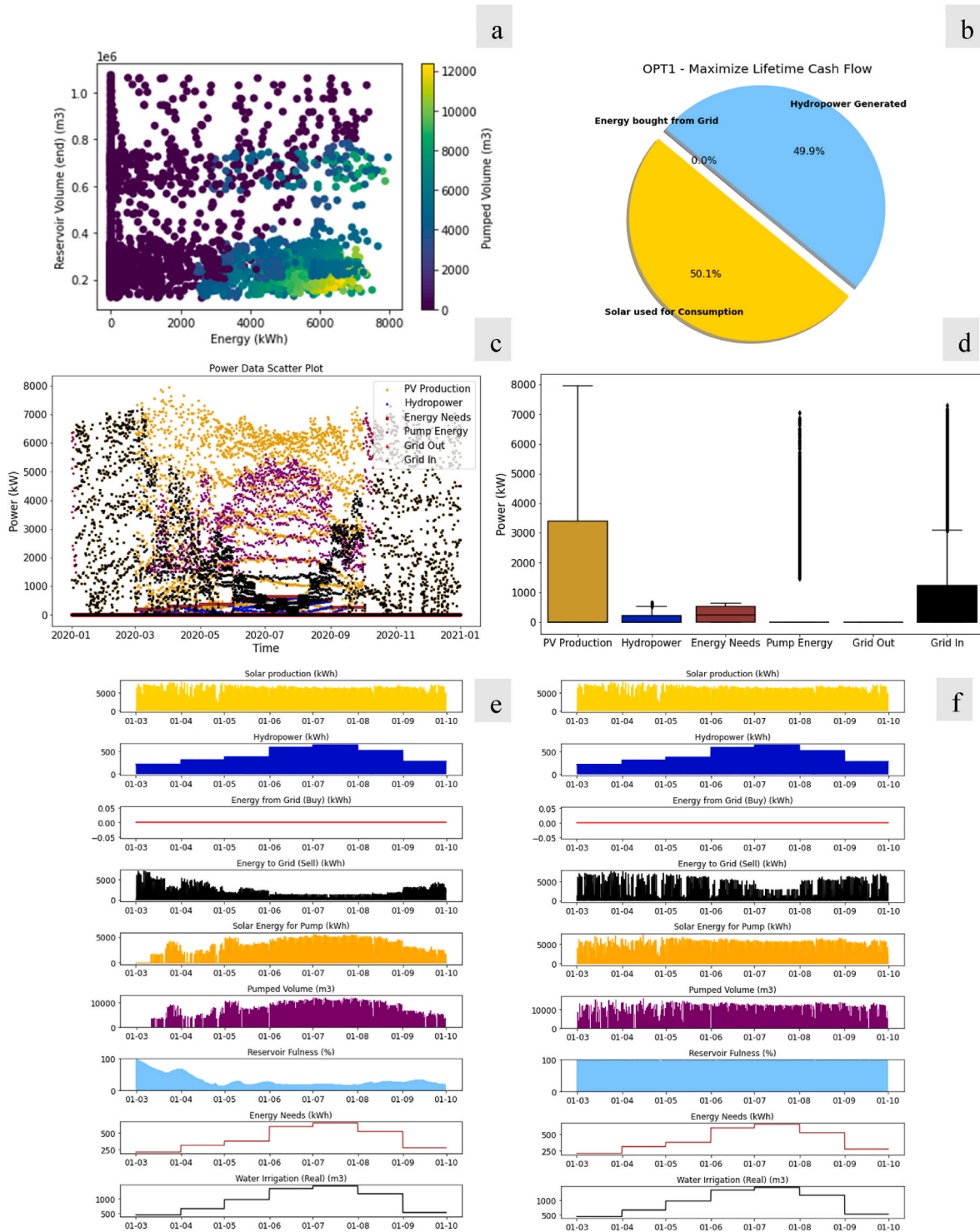
Fig. 7. Energy sources symbioses: (a) Solar and PHS relation; (b) Energy Needs distribution by source; (c) Distribution power data by source; (d) Power data by source; (e) Yearly energy balance OPT1; (f) Yearly energy balance OPT2 for 4.8 Mm^3 of water needs.

CRediT authorship contribution statement

JoaoS.T. Coelho: Investigation, Formal analysis. **Modesto Pérez-Sánchez:** Writing – review & editing, Writing – original draft, Funding acquisition, Conceptualization. **Oscar E. Coronado-Hernández:** Writing – original draft, Software. **Mohsen Besharat:** Validation, Software. **Rui-Lin Feng:** Visualization. **Elias Tasca:** Formal analysis. **Ling Zhou:** Writing – original draft. **Helena M. Ramos:** Writing – review & editing, Writing – original draft, Validation, Supervision, Methodology, Conceptualization.

Declaration of competing interest

The authors declare that they have no known competing financial interests or personal relationships that could have appeared to influence the work reported in this paper.

Acknowledgments

Appendix A. Supplementary data

Supplementary data to this article can be found online at https://doi.org/10.1016/j.rineng.2024.103117.

Data availability

Data will be made available on request.

References

[1] P. Roos, A. Haselbacher, Analytical modeling of advanced adiabatic compressed air energy storage: literature review and new models, Renew. Sustain. Energy Rev. 163 (2022) 112464, https://doi.org/10.1016/j.rser.2022.112464.

[2] N. Świdyńska, Renewable energy sources in Poland in 2014-2023 and the perspective of their development until 2030. A contribution to the discussion, Olsztyn Econ. J. 19 (2024) 31–44, https://doi.org/10.31648/OEJ.10093.

[3] Q. Hassan, P. Viktor, T. J Al-Musawi, B. Mahmood Ali, S. Algburi, H.M. Alzoubi, A. Khudhair Al-Jiboory, A. Zuhair Sameen, H.M. Salman, M. Jaszczur, The renewable energy role in the global energy Transformations, Renew. Energy Focus 48 (2024) 100545, https://doi.org/10.1016/J.REF.2024.100545.

[4] Y. Ghorbani, S.E. Zhang, G.T. Nwaila, J.E. Bourdeau, D.H. Rose, Embracing a diverse approach to a globally inclusive green energy transition: moving beyond decarbonisation and recognising realistic carbon reduction strategies, J. Clean. Prod. 434 (2024) 140414, https://doi.org/10.1016/J.JCLEPRO.2023.140414.

[5] S.O. Rey, J.A. Romero, L.T. Romero, À.F. Martínez, X.S. Roger, M.A. Qamar, J. L. Domínguez-García, L. Gevorkov, Powering the future: a comprehensive review of battery energy storage systems, Energies 16 (2023).

[6] A. Saldarini, M. Longo, M. Brenna, D. Zaninelli, Battery electric storage systems: advances, challenges, and market trends, Energies 16 (2023).

[7] P. Behera, L. Sethi, N. Sethi, Balancing India's energy trilemma: assessing the role of renewable energy and green technology innovation for sustainable development, Energy 308 (2024) 132842, https://doi.org/10.1016/J.ENERGY.2024.132842.

[8] O. Babaharra, K. Choukairy, H. Faraji, S. Hamdaoui, Improved heating floor thermal performance by adding PCM microcapsules enhanced by single and hybrid nanoparticles, Heat Transf 52 (2023) 3817–3838, https://doi.org/10.1002/htj.22853.

[9] E.M. Berra, M. Faraji, H. Faraji, Numerical simulation with LBM of the cooling of electronic component: effect of the inclination angle, Mater. Today Proc. 30 (2020) 838–841, https://doi.org/10.1016/j.matpr.2020.04.194.

[10] Y. Hariti, A. Hader, H. Faraji, Y. Boughaleb, Scaling law of permeability and porosity for fluid transport Phenomena in porous PCM media, J. Appl. Comput. Mech. 7 (2021) 84–92, https://doi.org/10.22055/jacm.2020.35136.2577.

[11] A.M. Rabi, J. Radulovic, J.M. Buick, Comprehensive review of compressed air energy storage (CAES) technologies, Thermo 3 (2023) 104–126.

[12] M. Jankowski, A. Pałac, K. Sornek, W. Goryl, M. Żołądek, M. Homa, M. Filipowicz, Status and development perspectives of the compressed air energy storage (CAES) technologies—a literature review, Energies 17 (2024).

[13] S.M. Alirahmi, T. Gundersen, A. Arabkoohsar, J.J. Klemeš, G. Sin, H. Yu, Process design, integration, and optimization of a novel compressed air energy storage for the coproduction of electricity, cooling, and water, Renew. Sustain. Energy Rev. 189 (2024) 114034, https://doi.org/10.1016/J.RSER.2023.114034.

[14] I. Nabil, M. Mohamed Khairat Dawood, T. Nabil, Review of energy storage technologies for compressed-air energy storage, Am. J. Mod. Energy 7 (2021) 51, https://doi.org/10.11648/j.ajme.20210704.12.

[15] T.S. Le, T.N. Nguyen, D.-K. Bui, T.D. Ngo, Optimal sizing of renewable energy storage: a techno-economic analysis of hydrogen, battery and hybrid systems considering degradation and seasonal storage, Appl. Energy 336 (2023) 120817, https://doi.org/10.1016/j.apenergy.2023.120817.

[16] Z. Ren, H. Li, W. Yan, W. Lv, G. Zhang, L. Lv, L. Sun, Z. Sun, W. Gao, Comprehensive evaluation on production and recycling of lithium-ion batteries: a critical review, Renew. Sustain. Energy Rev. 185 (2023) 113585, https://doi.org/10.1016/J.RSER.2023.113585.

[17] A.G. Olabi, Q. Abbas, P.A. Shinde, M.A. Abdelkareem, Rechargeable batteries: technological advancement, challenges, current and emerging applications, Energy 266 (2023) 126408, https://doi.org/10.1016/J.ENERGY.2022.126408.

[18] W. Jan, A.D. Khan, F.J. Iftikhar, G. Ali, Recent advancements and challenges in deploying lithium sulfur batteries as economical energy storage devices, J. Energy Storage 72 (2023) 108559, https://doi.org/10.1016/J.EST.2023.108559.

[19] M. Heidari, M. Heidari, A. Soleimani, B. Mehdizadeh Khorrami, A. Pinnarelli, P. Vizza, M. Dzikuć, Techno-economic optimization and Strategic assessment of sustainable energy solutions for Powering remote communities, Results Eng 23 (2024) 102521, https://doi.org/10.1016/j.rineng.2024.102521.

[20] I. Kougias, T. Patsialis, A. Zafirakou, N. Theodossiou, Exploring the potential of energy recovery using micro hydropower systems in water supply systems, Water Util. J 7 (2014) 25–33.

[21] H.M. Ramos, O.E. Coronado-Hernández, P.A. Morgado, M. Simão, Mathematic modelling of a reversible hydropower system: dynamic effects in turbine mode, Water 15 (2023).

[22] M. Simão, H.M. Ramos, Hybrid pumped hydro storage energy solutions towards wind and PV integration: improvement on flexibility, reliability and energy costs, Water 12 (2020).

[23] A. Borg, T. Sant, D. Buhagiar, R.N. Farrugia, C. Micallef, A numerical model comparison of the energy conversion process for an offshore hydro-pneumatic energy storage system, Appl. Sci. 13 (2023), https://doi.org/10.3390/APP13127189.

[24] A.T.D. Perera, K. Javanroodi, D. Mauree, V.M. Nik, P. Florio, T. Hong, D. Chen, Challenges resulting from urban density and climate change for the EU energy transition, Nat. Energy 84 (8) (2023) 397–412, https://doi.org/10.1038/s41560-023-01232-9, 2023.

[25] A. M, P.K. G, Hydrogen towards sustainable transition: a review of production, economic, environmental impact and scaling factors, Results Eng 20 (2023) 101456, https://doi.org/10.1016/J.RINENG.2023.101456.

[26] M.I. El-Afifi, B.E. Sedhom, A.A. Eladl, M. Elgamal, P. Siano, Demand side management strategy for smart building using multi-objective hybrid optimization technique, Results Eng 22 (2024) 102265, https://doi.org/10.1016/J.RINENG.2024.102265.

[27] M. Farghali, A.I. Osman, I.M.A. Mohamed, Z. Chen, L. Chen, I. Ihara, P.S. Yap, D. W. Rooney, Strategies to Save Energy in the Context of the Energy Crisis: a Review, vol. 21, Springer International Publishing, 2023.

[28] H.M. Ramos, M.P. Amaral, D.I.C. Covas, Pumped-storage solution towards energy efficiency and sustainability: Portugal contribution and real case studies, J. Water Resour. Prot. 6 (2014) 1099–1111, https://doi.org/10.4236/JWARP.2014.612103.

[29] J. Joo, J. Paavola, J. Van Alstine, Contested net-zero target setting in a transitioning country: the case of South Korea, Futures 147 (2023) 103114, https://doi.org/10.1016/J.FUTURES.2023.103114.

[30] J. Tian, L. Yu, R. Xue, S. Zhuang, Y. Shan, Global low-carbon energy transition in the post-COVID-19 era, Appl. Energy 307 (2022) 118205, https://doi.org/10.1016/J.APENERGY.2021.118205.

[31] F. Rozon, C. McGregor, M. Owen, Long-term forecasting framework for renewable energy technologies' installed capacity and costs for 2050, Energies 16 (2023).

[32] M. Laimon, S. Goh, Unlocking potential in renewable energy curtailment for green ammonia production, Int. J. Hydrogen Energy 71 (2024) 964–971, https://doi.org/10.1016/J.IJHYDENE.2024.05.022.

[33] P. Li, Z. Zhao, J. Li, Z. Liu, Y. Liu, M.A. Mahmud, Y. Sun, D. Chen, Unlocking potential contribution of seasonal pumped storage to ensure the flexibility of power systems with high proportion of renewable energy sources, Renew. Energy 218 (2023) 119280, https://doi.org/10.1016/J.RENENE.2023.119280.

[34] T.K. Yuguda, S.A. Imanche, T. Ze, T.Y. Akintunde, B.S. Luka, Hydropower development, policy and partnership in the 21st century: a China-Nigeria outlook, Energy Environ. 34 (2022) 1170–1204, https://doi.org/10.1177/0958305X221079423.

[35] T. Levin, J. Bistline, R. Sioshansi, W.J. Cole, J. Kwon, S.P. Burger, G.W. Crabtree, J. D. Jenkins, R. O'Neil, M. Korpås, et al., Energy storage solutions to decarbonize electricity through enhanced capacity expansion modelling, Nat. Energy (8) (2023) 1199–1208, https://doi.org/10.1038/s41560-023-01340-6.

[36] K.E. Gan, O. Taikan, T.Y. Gan, T. Weis, D. Yamazaki, H. Schüttrumpf, Enhancing renewable energy systems, contributing to sustainable development goals of united nation and building resilience against climate change impacts, Energy Technol. 11 (2023) 2300275, https://doi.org/10.1002/ENTE.202300275.

[37] A.P. Alonso, Pumped hydro energy storage systems for a sustainable energy planning, Sustain. Energy Plan. Smart Grids (2024) 71–89, https://doi.org/10.1016/B978-0-443-14154-6.00014-4.

[38] B.A. Bhatti, S. Hanif, J. Alam, B. Mitra, R. Kini, D. Wu, Using energy storage systems to extend the life of hydropower plants, Appl. Energy 337 (2023) 120894, https://doi.org/10.1016/J.APENERGY.2023.120894.

[39] Z. Wang, G. Fang, X. Wen, Q. Tan, P. Zhang, Z. Liu, Coordinated operation of conventional hydropower plants as hybrid pumped storage hydropower with wind and photovoltaic plants, Energy Convers. Manag. 277 (2023) 116654, https://doi.org/10.1016/J.ENCONMAN.2022.116654.

[40] P.C. Nikolaos, F. Marios, K. Dimitris, A review of pumped hydro storage systems, Energies 16 (2023).

[41] R. GhoshThakur, R. Dhar Ruchi, A. Ghosh, S. GonChaudhuri, S. Balachandran, Green inertia and reliable power: fortifying edge-to-grid connectivity with micro variable speed solar pumped storage, Energy Convers. Manag. 307 (2024) 118375, https://doi.org/10.1016/J.ENCONMAN.2024.118375.

[42] M. Amir, R.G. Deshmukh, H.M. Khalid, Z. Said, A. Raza, S.M. Muyeen, A.S. Nizami, R.M. Elavarasan, R. Saidur, K. Sopian, Energy storage technologies: an integrated survey of developments, global economical/environmental effects, optimal scheduling model, and sustainable adaption policies, J. Energy Storage 72 (2023) 108694, https://doi.org/10.1016/J.EST.2023.108694.

[43] J. Qiu, J. Zhao, F. Wen, J. Zhao, C. Gao, Y. Zhou, Y. Tao, S. Lai, Challenges and pathways of low-carbon oriented energy transition and power system planning strategy: a review, IEEE Trans. Netw. Sci. Eng. (2023), https://doi.org/10.1109/TNSE.2023.3344729.

[44] R. Dindorf, J. Takosoglu, P. Wos, Review of hydro-pneumatic accumulator models for the study of the energy efficiency of hydraulic systems, Energies 16 (2023), https://doi.org/10.3390/EN16186472.

[45] J.T. Putra, Sarjiya, M.I.B. Setyonegoro, Modeling of high uncertainty photovoltaic generation in quasi dynamic power flow on distribution systems: a case study in Java Island, Indonesia, Results Eng 21 (2024) 101747, https://doi.org/10.1016/j.rineng.2023.101747.

[46] J.S.T. Coelho, M. van de Loo, J.A. Díaz, O.E. Coronado-Hernández, M. Perez-Sanchez, H.M. Ramos, Multi-objective and multi-variable optimization models of hybrid renewable energy solutions for water–energy nexus, Water 16 (2024).

[47] M. Besharat, O.E. Coronado-Hernández, V.S. Fuertes-Miquel, M.T. Viseu, H. M. Ramos, Backflow air and pressure analysis in emptying a pipeline containing an entrapped air pocket, Urban Water J. 15 (2018) 769–779, https://doi.org/10.1080/1573062X.2018.1540711.

[48] H. Ramos, A.B. Almeida, Dynamic orifice model on waterhammer analysis of high or medium heads of small hydropower schemes, J. Hydraul. Res. 39 (2001) 429–436, https://doi.org/10.1080/00221680109499847.

[49] H.M. Ramos, V.S. Fuertes-Miquel, E. Tasca, O.E. Coronado-Hernández, M. Besharat, L. Zhou, B. Karney, Concerning dynamic effects in pipe systems with two-phase flows: pressure surges, cavitation, and ventilation, Water 14 (2022).

[50] X. Fu, S. Fu, C. Liu, M. Zhang, Q. Hu, Data-driven approach for modeling Reynolds stress tensor with invariance preservation, Comput. Fluids 274 (2024) 106215, https://doi.org/10.1016/J.COMPFLUID.2024.106215.

[51] M. Aydogdu, Analysis of the effect of rigid vegetation patches on the hydraulics of an open channel flow with Realizable k-ε and Reynolds stress turbulence models, Flow Meas. Instrum. 94 (2023) 102477, https://doi.org/10.1016/J.FLOWMEASINST.2023.102477.

[52] S. Ayele, Z.G. Workneh, B.T. Meshesha, Water challenges of Dire Dawa city of Ethiopia: an assessment of urban growth and groundwater supply, Environ. Challenges 12 (2023) 100738, https://doi.org/10.1016/J.ENVC.2023.100738.

[53] M.J. Moran, H.N. Shapiro, Fundamentals of Engineering Thermodynamics, 18, 1993.

[54] H.M. Ramos, B. Vargas, J.R. Saldanha, New integrated energy solution idealization: hybrid for renewable energy network (Hy4REN), Energies 15 (2022).

[55] S. Fontanella, O. Fecarotta, B. Molino, L. Cozzolino, R. Della Morte, A performance prediction model for pumps as turbines (PATs), Water 12 (2020).

[56] D.A. Paternina-Verona, L.C. Flórez-Acero, O.E. Coronado-Hernández, H. G. Espinoza-Román, V.S. Fuertes-Miquel, H.M. Ramos, Two-dimensional simulation of emptying manoeuvres in water pipelines with admitted air, Urban Water J. 20 (2023) 801–812, https://doi.org/10.1080/1573062X.2023.2211053.